ChemComm

COMMUNICATION

View Article Online
View Journal | View Issue

Cite this: *Chem. Commun.*, 2017, 53, 12004

Received 23rd August 2017,
Accepted 9th October 2017

DOI: 10.1039/c7cc06615e

rsc.li/chemcomm

Highly efficient Cs-based perovskite light-emitting diodes enabled by energy funnelling†

Yan Fong Ng,[abc] Sneha A. Kulkarni,[a] Shayani Parida,[d] Nur Fadilah Jamaludin,[abc] Natalia Yantara,[a] Annalisa Bruno,[a] Cesare Soci,[e] Subodh Mhaisalkar[ac] and Nripan Mathews *[ac]

The incorporation of phenylethylammonium bromide (PEABr) into a fully inorganic $CsPbBr_3$ perovskite framework led to the formation of mixed-dimensional perovskites, which enhanced the photoluminescence due to efficient energy funnelling and morphological improvements. With a PEABr : $CsPbBr_3$ ratio of 0.8 : 1, PeLEDs with a current efficiency of 6.16 cd A^{-1} and an EQE value of 1.97% have been achieved.

Halide perovskites have established themselves as a strong contender for state-of-the-art organic and quantum dot LEDs, due to their long-ranged electron and hole diffusion lengths,[1] tunable band gap, high colour purity and low deep trap defect density,[2,3] along with low material cost and solution processability. However, three-dimensional (3D) perovskites ($CH_3NH_3PbX_3$, where X = I, Br or Cl) suffer from low photoluminescence quantum yield (PLQY) as a result of small exciton binding energy that leads to a low radiative recombination rate.[4] This is compounded by trap state densities which are relevant at low injected carrier densities leading to non-radiative recombination.[5,6] To overcome this, quasi-2D perovskite structures have been explored by intercalating large organic counter-cations within the lead halide networks.[7,8] By tuning the ratio of 2D to 3D composition, the energy landscape can be tailored such that the charge carriers can be funnelled and concentrated in the lowest band gap (3D) radiative domains efficiently. The artificial concentration of carriers in the 3D system allows traps to be quickly filled up, thereby enhancing radiative recombination and achieving higher PLQY along with improved device performance.[9–11] However, all reported literature data on quasi-2D perovskite light-emitting diodes (PeLEDs) have been based on hybrid systems comprising organic cations, which are well known to have poor thermal stability.[12,13] By substituting the organic cation with a fully inorganic one (*e.g.* Cs), the perovskite material's resistance against thermal and ambient degradation can be greatly augmented.[14] Despite this, issues with $CsPbBr_3$ perovskite include even lower exciton binding energy (40 meV),[15] and poor morphological structures as a result of low precursor solubility and limitations in anti-solvent approaches.[16,17] The combination of these stumbling blocks resulted in shunt paths and non-radiative recombination losses. Various approaches such as interfacial engineering have improved the current efficiency to 2.9 cd A^{-1} and maximum luminance (L_{max}) to 10 700 cd m^{-2};[18] while a dual-phase nanoparticle composite film has also shown better control over the trap density, yielding devices with a current efficiency of 8.98 cd A^{-1} and an L_{max} value of 3853 cd m^{-2}.[19]

In this work, we show that the incorporation of a large alkylated bromide molecule into the framework of a fully inorganic $CsPbBr_3$ 3D perovskite film yields remarkable improvement in the photophysical and morphological properties. By carefully tuning the molar addition of PEABr, highly uniform, smooth and nano-sized grains were achieved with efficient energy channelling through an energy cascade as proven by various spectroscopic analyses. The benefits are well reflected in PeLEDs made from this quasi-2D mix, giving more than fifty-fold increment in luminance and efficiency.

The $CsPbBr_3$ precursor was prepared using excess of CsBr as previously reported.[16] The perovskite solutions with excess of PEABr addition were prepared in different molar ratios, *i.e.* PEABr : $CsPbBr_3$ = 0 : 1, 0.05 : 1, 0.1 : 1, 0.2 : 1, 0.3 : 1, 0.5 : 1, 0.8 : 1 and 1 : 1 to study the effect of PEABr addition. The typical absorption (Fig. 1a and Fig. S1, ESI†) peak onset at 525 nm (band gap = 2.34 eV)[20] for the 3D $CsPbBr_3$ perovskite was noted for all films prepared with the addition of different amounts of PEABr. Interestingly, the films formed with PEABr : $CsPbBr_3$ ratios above 0.2 : 1 were found to exhibit secondary absorption peaks at lower wavelengths (*e.g.* 450 nm), which are attributed to quasi-2D excitonic absorption. With further addition of PEABr,

[a] *Energy Research Institute@NTU (ERI@N), Research Techno Plaza, X-Frontier Block, Level 5, 50 Nanyang Drive, 637553, Singapore*
[b] *Interdisciplinary Graduate School, Nanyang Technological University, 50 Nanyang Avenue, 639798, Singapore*
[c] *School of Materials Science and Engineering, Nanyang Technological University, 50 Nanyang Avenue, 639798, Singapore. E-mail: Nripan@ntu.edu.sg*
[d] *Indian Institute of Science, CV Raman Road, Bengaluru, Karnataka 560012, India*
[e] *Division of Physics and Applied Physics, School of Physical and Mathematical Sciences, Nanyang Technological University, 21 Nanyang Link, 637371, Singapore*
† Electronic supplementary information (ESI) available. See DOI: 10.1039/c7cc06615e

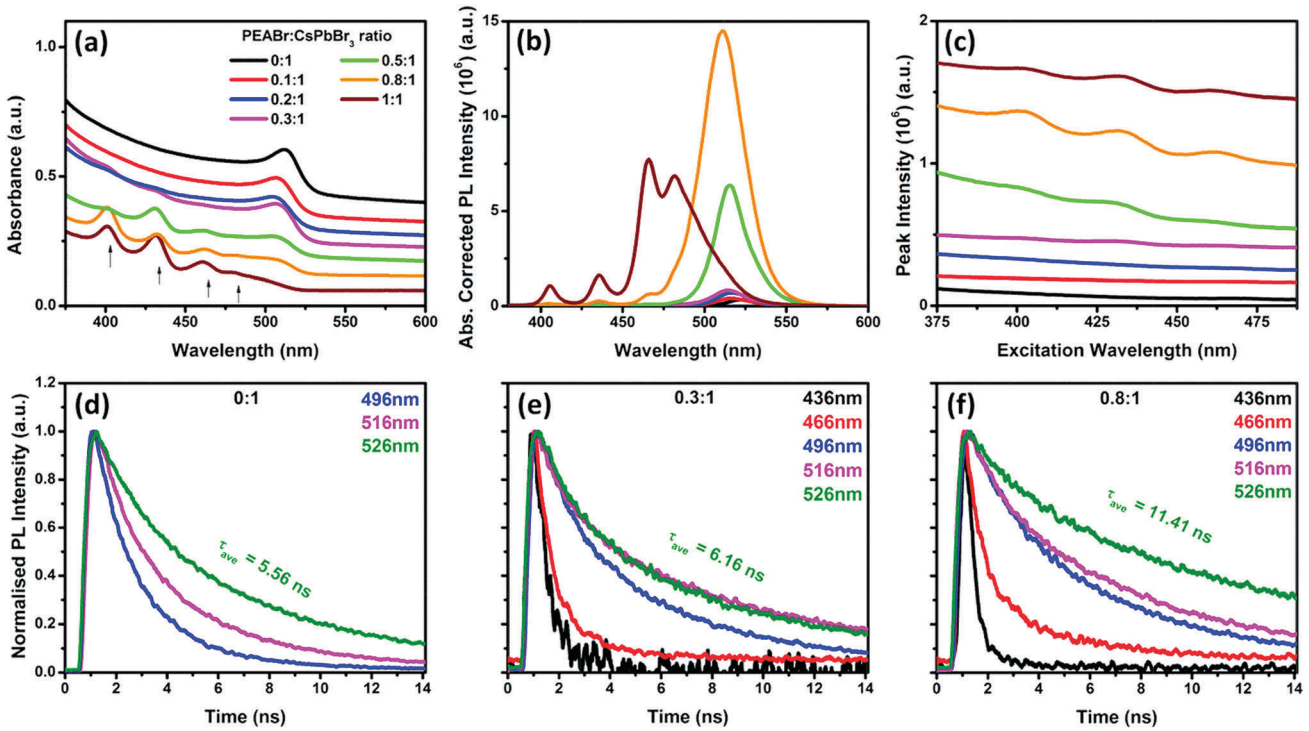

Fig. 1 (a) UV-visible absorption (plotted with a constant offset; arrow indicates the absorption peak due to quasi-2D/2D perovskite formation), (b) PL (absorbance corrected), and (c) excitation spectra (plotted with a constant offset) of $CsPbBr_3$ perovskite films prepared with the addition of different molar excesses of PEABr. (d–f) TRPL spectra for (d) pristine $CsPbBr_3$, (e) PEABr : $CsPbBr_3$ = 0.3 : 1, and (f) PEABr : $CsPbBr_3$ = 0.8 : 1 perovskite films. The colour of the curves (d–f) corresponds to the specific wavelengths measured as shown in respective graphs. All perovskites films were deposited on glass substrates for optical measurements.

the quasi-2D absorption becomes more dominant with the attenuation of the 3D peak, indicating a transition from 3D towards a more layered perovskite structure. The absorption peak at ~400 nm corresponds to a pure 2D $(PEA)_2PbBr_4$ phase ($n = 1$)[10,21] whereas the other peaks (centred at ~430, 460 and 480 nm) are signatures of layered perovskites with $n = 2, 3, 4$ or higher order.[22,23] At the 1 : 1 ratio, the 3D absorption is almost absent, implying that the film is mainly composed of quasi-2D phases. With increasing PEABr : $CsPbBr_3$ ratios up to 0.8 : 1, an enhancement in the absorbance-corrected PL intensity (Fig. 1b and Fig. S2, ESI†) is observed. The majority of the emission originates mainly from the 3D perovskite phase (511–522 nm), corresponding to the band gap of 2.34 eV, which is lower than those of the quasi-2D (~2.78 eV) and pure 2D (~3.06 eV) phases. The huge enhancement in the PL intensity of the 0.8 : 1 quasi-2D perovskite is likely due to (i) efficient funnelling of the photoexcitation energy and (ii) spatial charge confinement due to morphological improvement, both of which will be verified subsequently. It is also possible that the larger PEA cations can passivate defects at lattice surfaces and grain boundaries as speculated by Jen and co-workers,[24] thereby reducing shunt paths and non-radiative recombination losses. From the normalized PL spectra (Fig. S3, ESI†), gradual blue-shifts in the PL peak position with increasing PEABr : $CsPbBr_3$ ratio was observed from 522 nm (0 : 1) to 511 nm (0.8 : 1) due to the reduced domains of the perovskite structure. At ratios of 0.2 : 1 and above, additional PL emission with low but appreciable intensities are detected at wavelengths of 483 nm, 467 nm, 436 nm and 405 nm. These extra peaks are attributed to the reduced dimensionality of the perovskite[4] and are closely in line with the quasi-2D absorption signatures. At a higher ratio of 1 : 1, however, the emission from the 3D perovskite (~511 nm) becomes diminished while the quasi-2D emission dominates due to the formation of more layered perovskite phases. Following the PL spectra, all samples emitted green light under UV excitation except the 1 : 1 sample which gave a bluish-green tinge (Fig. S4, ESI†).

While the additional quasi-2D emission peaks at lower wavelengths may affect the purity of the emitted light, they could be beneficial in fine-tuning the energy landscape and revamping the behaviour of the charge carriers.[9,11] In order to investigate this effect, the PL excitation spectra were recorded (Fig. 1c). For the pure $CsPbBr_3$ film, there is no significant contribution to the emission below 500 nm. However, for the PEABr : $CsPbBr_3$ samples, the signature peaks of the quasi-2D structure can be observed in the excitation spectra starting from PEABr ratios as low as 0.3 : 1, with more obvious magnitudes at ratios of 0.5 : 1 and above. The presence of these peaks implies that the quasi-2D domains (larger band gap) significantly contribute to the emission of the 3D phase due to the efficient energy funnelling from the larger band gap to the lower band gap domains. The funnelling effect is further probed by a systematic wavelength dependent study of time-resolved PL (TRPL) decays as shown in Fig. 1d–f. The TRPL decays are well described by a bi-exponential decay function comprising a fast component (either due to presence of defects or due to energy transfer processes),

related to non-radiative recombination processes, and a slow decay component related to the radiative recombination.[10,25] Both the characteristic decay times and the calculated average lifetime values are tabulated in Table S1 (ESI†). The TRPL decays were measured for various emission wavelengths corresponding to the peaks observed in the steady-state PL emission (Fig. 1e and f). The measured lifetimes strongly depend on the emission wavelength, consistent with the different natures of the 2D and 3D domains present in the samples.[9] Indeed, the lifetime increases by almost one order of magnitude from hundreds of ps to a few ns across the different emission wavelengths (in both samples with 0.3 : 1 and 0.8 : 1 ratios), consistently in line with the presence of different structures. Even more interestingly, by comparing the fluorescence lifetime at the same emission wavelength across the different samples, it is observed that with increasing PEABr content, the decay of the 2D phase becomes slightly faster (436 nm signal) while the 3D component (526 nm) becomes significantly longer (*e.g.* from 5.56 ns in $CsPbBr_3$ to 6.16 ns in 0.3 : 1 and 11.41 ns in the 0.8 : 1 sample), suggesting that the energy transfer to the 3D domains increases the carrier density in these domains, thereby overwhelming the charge carrier trap states. The lifetimes also confirm that the highest radiative recombination occurs with the addition of 80 mol% excess PEABr (ratio of 0.8 : 1), which is consistent with the highest PL intensity measured with this PEABr concentration (Fig. 1b).

The field emission scanning electron microscopy (FESEM) images of the pure $CsPbBr_3$ film show large and non-uniform grains with visible pinholes along with a rough top surface as seen from the cross-sectional image (Fig. 2a and d). At a PEABr : $CsPbBr_3$ ratio of 0.3 : 1, however, the grain size is reduced and fewer pinholes were observed (Fig. 2b and e). Beyond this ratio, the quasi-2D films become pinhole-free (Fig. S5 and S6, ESI†). With a ratio of 0.8 : 1, nano-sized grains with uniform and flat top surfaces were achieved (Fig. 2c and f). This morphological evolution can be explained by the fact that the bulky PEA chains could not fit inside the 3D lattice of $CsPbBr_3$,[26] thus they function as ligands that surround the 3D crystallites.[4] As a result, the growth of 3D perovskite grains becomes inhibited while layered structures are preferentially formed, leading to smaller grains and smoother films. These morphological refinements facilitate charge injection and confinement, and improve radiative recombination, which will be discussed in the next section. The X-ray diffraction (XRD) patterns (Fig. S7a, ESI†) show an orthorhombic (Pnma) crystal structure of $CsPbBr_3$, in agreement with the reported literature.[27] The XRD peak positions of $CsPbBr_3$ are invariant with PEABr addition, while the quasi-2D formation was confirmed in the XRD spectra of thicker films prepared *via* drop-casting (Fig. S7b, ESI†).

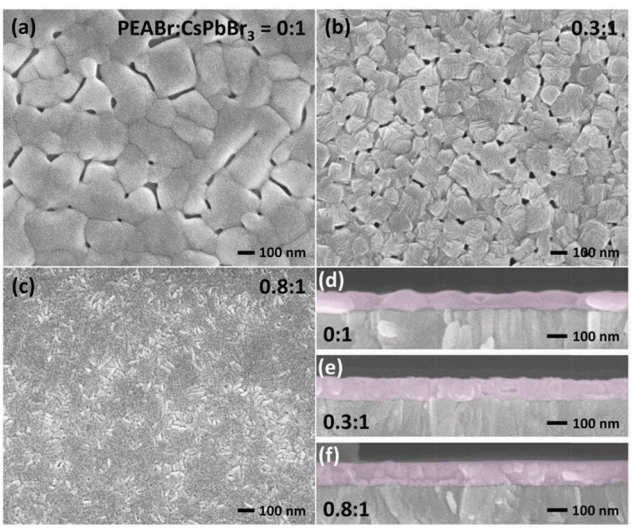

Fig. 2 FESEM images of $CsPbBr_3$ perovskite films prepared with different PEABr : $CsPbBr_3$ molar ratios, showing the surface morphology (a–c) and cross-sectional view (d–f). All perovskite films were deposited on ITO/PEDOT:PSS substrates.

PeLEDs (device architecture shown in the inset of Fig. 3b) were then fabricated and tested, with the resultant current density–voltage–luminance (*J–V–L*) and efficiency curves shown in Fig. 3a–c. The L_{max}, turn-on voltage (V_{th}), current efficiency, and external quantum efficiency (EQE) of the best and average devices are tabulated in Table S2 (ESI†). The pure $CsPbBr_3$ device only obtained a L_{max} of 271 cd m^{-2} while increasing the PEABr : $CsPbBr_3$ ratio to 0.2 : 1 and above achieved performances close to or greater than 10 000 cd m^{-2}. The V_{th} value was reduced from 4 V to 3 V after PEABr addition, while the current efficiency escalated rapidly from 0.13 cd A^{-1} to more than 1 cd A^{-1}. The best device was achieved at a PEABr : $CsPbBr_3$ ratio of 0.8 : 1, yielding a current efficiency of 6.16 cd A^{-1} and an EQE of 1.97%, which is ~50 times that of the pure $CsPbBr_3$. The substantial enhancement in device performance is attributable to the combinatorial effect of the charge dynamics and film morphology. The energy landscape created by the quasi-2D states (which is absent in the pure 3D perovskite) allows efficient energy transfer from the larger band gap to the smallest band gap region, thereby amplifying electron–hole capture and radiative recombination rates.[9] Concomitantly, the formation of a compact film with nano-sized grains is the key to suppressing leakage currents and spatially confine injected charge carriers.[28] These two effects contribute concurrently to achieve high luminance and better efficiency of the quasi-2D devices. Increasing uniformity and smoothness of the PEABr–$CsPbBr_3$ films also allow better interfacial contact with the electron transport layer, thereby reducing V_{th}. However, at a higher PEABr : $CsPbBr_3$ ratio of 1 : 1, the formation of the 3D perovskite phase becomes impeded (Fig. 1a), which considerably hinders the charge transport and reduces the emissive area, thereby resulting in a drop in the device performance.

Interestingly, the electroluminescence (EL) spectra show only single emission peaks for all devices (Fig. S8, ESI†), even at high biases (Fig. S9, ESI†). The peak positions closely match the lowest band gap PL wavelength of each film and no additional quasi-2D emission was observed, indicating the successful energy cascade and carrier confinement in the lowest band gap phase. All devices show narrowband green emission (inset of Fig. 3c) with a full width at half maximum ($FWHM_{EL}$) of 20–22 nm. The material system also displayed superior thermal stability compared to $CH_3NH_3PbBr_3$ thin films (Fig. S10, ESI†).

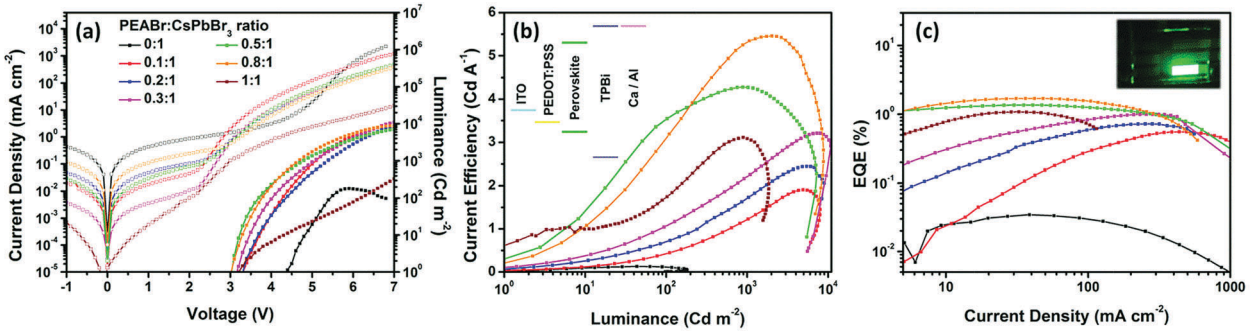

Fig. 3 (a) *J*–*V*–*L*, (b) current efficiency, and (c) EQE curves of PeLEDs fabricated with $CsPbBr_3$ perovskites prepared using different PEABr : $CsPbBr_3$ molar ratios. Inset of (b) shows the device architecture used while the inset of (c) shows an image of the 0.8 : 1 PeLED under an applied bias of 4 V.

To the best of our knowledge, this work presents the first study of a quasi-2D $CsPbBr_3$ based perovskite framework. The integration of PEABr and $CsPbBr_3$ in a mixed-dimensional configuration brings about a threefold benefit of (i) a smooth and pinhole-free film morphology, (ii) nano-sized grains, and (iii) constructive energy channelling towards the smallest band gap phase. The eventual outcome is the realization of highly luminous ($L_{max} > 10\,000$ cd m^{-2}) and efficient PeLEDs (current efficiency >6 cd A^{-1}, EQE $\approx$ 2%) with pure green emission ($FWHM_{EL} \sim 20$ nm). The methodology involved in this work is simple, allowing ample opportunity for large scale production.

This research was supported by the National Research Foundation, Prime Minister's Office, Singapore, under its Competitive Research Programme (CRP Award No. NRF-CRP14-2014-03) and MOE Tier 1 RG166/16.

Conflicts of interest

There are no conflicts to declare.

Notes and references

1 G. Xing, N. Mathews, S. Sun, S. S. Lim, Y. M. Lam, M. Grätzel, S. Mhaisalkar and T. C. Sum, *Science*, 2013, **342**, 344–347.
2 S. A. Veldhuis, P. P. Boix, N. Yantara, M. Li, T. C. Sum, N. Mathews and S. G. Mhaisalkar, *Adv. Mater.*, 2016, **28**, 6804–6834.
3 Y.-H. Kim, H. Cho and T.-W. Lee, *Proc. Natl. Acad. Sci. U. S. A.*, 2016, **113**, 11694–11702.
4 Z. Xiao, R. A. Kerner, L. Zhao, N. L. Tran, K. M. Lee, T.-W. Koh, G. D. Scholes and B. P. Rand, *Nat. Photonics*, 2017, **11**, 108–115.
5 G. Xing, N. Mathews, S. S. Lim, N. Yantara, X. Liu, D. Sabba, M. Grätzel, S. Mhaisalkar and T. C. Sum, *Nat. Mater.*, 2014, **13**, 476–480.
6 X. Wu, M. T. Trinh, D. Niesner, H. Zhu, Z. Norman, J. S. Owen, O. Yaffe, B. J. Kudisch and X. Y. Zhu, *J. Am. Chem. Soc.*, 2015, **137**, 2089–2096.
7 T. M. Koh, K. Thirumal, H. S. Soo and N. Mathews, *ChemSusChem*, 2016, **9**, 2541–2558.
8 N. Wang, L. Cheng, R. Ge, S. Zhang, Y. Miao, W. Zou, C. Yi, Y. Sun, Y. Cao, R. Yang, Y. Wei, Q. Guo, Y. Ke, M. Yu, Y. Jin, Y. Liu, Q. Ding, D. Di, L. Yang, G. Xing, H. Tian, C. Jin, F. Gao, R. H. Friend, J. Wang and W. Huang, *Nat. Photonics*, 2016, **10**, 699–704.
9 M. Yuan, L. N. Quan, R. Comin, G. Walters, R. Sabatini, O. Voznyy, S. Hoogland, Y. Zhao, E. M. Beauregard, P. Kanjanaboos, Z. Lu, D. H. Kim and E. H. Sargent, *Nat. Nano*, 2016, **11**, 872–877.
10 J. Byun, H. Cho, C. Wolf, M. Jang, A. Sadhanala, R. H. Friend, H. Yang and T.-W. Lee, *Adv. Mater.*, 2016, **28**, 7515–7520.
11 L. N. Quan, Y. Zhao, F. P. García de Arquer, R. Sabatini, G. Walters, O. Voznyy, R. Comin, Y. Li, J. Z. Fan, H. Tan, J. Pan, M. Yuan, O. M. Bakr, Z. Lu, D. H. Kim and E. H. Sargent, *Nano Lett.*, 2017, **17**, 3701–3709.
12 B. Conings, J. Drijkoningen, N. Gauquelin, A. Babayigit, J. D'Haen, L. D'Olieslaeger, A. Ethirajan, J. Verbeeck, J. Manca, E. Mosconi, F. D. Angelis and H.-G. Boyen, *Adv. Energy Mater.*, 2015, **5**, 1500477.
13 T. A. Berhe, W.-N. Su, C.-H. Chen, C.-J. Pan, J.-H. Cheng, H.-M. Chen, M.-C. Tsai, L.-Y. Chen, A. A. Dubale and B.-J. Hwang, *Energy Environ. Sci.*, 2016, **9**, 323–356.
14 M. Kulbak, S. Gupta, N. Kedem, I. Levine, T. Bendikov, G. Hodes and D. Cahen, *J. Phys. Lett.*, 2016, **7**, 167–172.
15 L. Protesescu, S. Yakunin, M. I. Bodnarchuk, F. Krieg, R. Caputo, C. H. Hendon, R. X. Yang, A. Walsh and M. V. Kovalenko, *Nano Lett.*, 2015, **15**, 3692–3696.
16 N. Yantara, S. Bhaumik, F. Yan, D. Sabba, H. A. Dewi, N. Mathews, P. P. Boix, H. V. Demir and S. Mhaisalkar, *J. Phys. Lett.*, 2015, **6**, 4360–4364.
17 Y. F. Ng, N. F. Jamaludin, N. Yantara, M. Li, V. K. R. Irukuvarjula, H. V. Demir, T. C. Sum, S. Mhaisalkar and N. Mathews, *ACS Omega*, 2017, **2**, 2757–2764.
18 X. Zhang, W. Wang, B. Xu, S. Liu, H. Dai, D. Bian, S. Chen, K. Wang and X. W. Sun, *Nano Energy*, 2017, **37**, 40–45.
19 X. Zhang, B. Xu, J. Zhang, Y. Gao, Y. Zheng, K. Wang and X. W. Sun, *Adv. Funct. Mater.*, 2016, **26**, 4595–4600.
20 E. M. L. D. de Jong, G. Yamashita, L. Gomez, M. Ashida, Y. Fujiwara and T. Gregorkiewicz, *J. Phys. Chem. C*, 2017, **121**, 1941–1947.
21 D. Liang, Y. Peng, Y. Fu, M. J. Shearer, J. Zhang, J. Zhai, Y. Zhang, R. J. Hamers, T. L. Andrew and S. Jin, *ACS Nano*, 2016, **10**, 6897–6904.
22 L. N. Quan, M. Yuan, R. Comin, O. Voznyy, E. M. Beauregard, S. Hoogland, A. Buin, A. R. Kirmani, K. Zhao, A. Amassian, D. H. Kim and E. H. Sargent, *J. Am. Chem. Soc.*, 2016, **138**, 2649–2655.
23 S. Bhaumik, S. A. Veldhuis, Y. F. Ng, M. Li, S. K. Muduli, T. C. Sum, B. Damodaran, S. Mhaisalkar and N. Mathews, *Chem. Commun.*, 2016, **52**, 7118–7121.
24 N. Li, Z. Zhu, C.-C. Chueh, H. Liu, B. Peng, A. Petrone, X. Li, L. Wang and A. K. Y. Jen, *Adv. Energy Mater.*, 2017, **7**, 1601307.
25 P.-W. Liang, C.-Y. Liao, C.-C. Chueh, F. Zuo, S. T. Williams, X.-K. Xin, J. Lin and A. K. Y. Jen, *Adv. Mater.*, 2014, **26**, 3748–3754.
26 D. B. Mitzi, S. Wang, C. A. Feild, C. A. Chess and A. M. Guloy, *Science*, 1995, **267**, 1473–1476.
27 C. C. Stoumpos, C. D. Malliakas, J. A. Peters, Z. Liu, M. Sebastian, J. Im, T. C. Chasapis, A. C. Wibowo, D. Y. Chung, A. J. Freeman, B. W. Wessels and M. G. Kanatzidis, *Cryst. Growth Des.*, 2013, **13**, 2722–2727.
28 H. Cho, S.-H. Jeong, M.-H. Park, Y.-H. Kim, C. Wolf, C.-L. Lee, J. H. Heo, A. Sadhanala, N. Myoung, S. Yoo, S. H. Im, R. H. Friend and T.-W. Lee, *Science*, 2015, **350**, 1222–1225.